https://dx.doi.org/10.1016/j.seta.2022.102344

Dynamic behavior of high-temperature CO_2/H_2O co-electrolysis coupled with real fluctuating renewable power

Yi Sun[1], Wenjin Zheng[1], Shiyu Ji[1], Anwei Sun[2, **], Wei Shuai[2], Nan Zheng[2], Yu Han[2], Gang Xiao[2], Meng Ni[3], Haoran Xu[2, *, **]

[1] Power China Huadong Engineering Co. Ltd., Hangzhou 310014, PR China

[2] State Key Laboratory of Clean Energy Utilization, Zhejiang University, 38 Zheda Road, Hangzhou, 310027, China

[3] Department of Building and Real Estate, Research Institute for Sustainable Urban Development (RISUD) & Research Institute for Smart Energy (RISE), Hong Kong Polytechnic University, Hung Hom, Kowloon, Hong Kong, China

Abstract: Direct utilization of fluctuational renewable powers leads to rapid changes of working conditions and brings difficulties in the operation of solid oxide electrolysis cells (SOECs). Herein, a multi-physics SOEC model is established to investigate its dynamic characteristics using a real photovoltaic power supply for co-electrolysis of H_2O and CO_2. Dynamic responses of key performances including the current density, the average SOEC temperature, the H_2O/CO_2 conversion rate and the output H_2/CO ratio are analyzed over a whole day. It is found that a high CO_2 mole fraction can help inhibit average temperature fluctuation, where the maximum temperature difference decreases from 110 to 57 K with the inlet CO_2 mole fraction increasing from 0.2 to 0.8. Besides, the largest temperature gradient occurs in the middle of the cell in the morning and gradually migrates to the inlet. Generally, a high inlet gas temperature can increase the outlet H_2/CO ratio especially at low voltages. The outlet H_2/CO ratio is also found to be closely related with the gas utilization rate, where a utilization rate of 0.6 shows 10% higher H_2/CO ratio than that of 0.8. This study can provide a guideline for the performance optimization of SOECs with fluctuating power supply.

Keywords: Solid oxide electrolysis cell; Co-electrolysis; Renewable energy storage; Numerical simulation; Dynamic characteristic.

*Corresponding author Email: haoranxu@zju.edu.cn (Haoran Xu)

**The two authors have the same contribution to this study.

1. Introduction

With a global determination to achieve a carbon-neutral society, the construction of renewable powers is boosting all over the world [1, 2]. Direct utilization of renewable power is limited by its highly intermittent nature, energy storage technologies such as are thus needed to convert the fluctuating energy into stable forms for subsequent use [3]. Electrochemical devices are alternative choices as they can provide a reversible route between electricity and fuels, where solid oxide electrolysis cell (SOEC) has attracted wide attentions [4].

SOEC is an all-solid device with a ceramic O^{2-}-conductive electrolyte sandwiched between two porous electrodes. It works at a high temperature (> 600 ^{o}C) and thus owns significant thermodynamic (high efficiency) and kinetic (high reaction activity) advantages. These advantages further allow the use of non-noble catalyst (e.g., Ni, Ag, Cu) and brings wide choices of reactants. Compared with low temperature electrolyzers, SOEC is of special interest as it can efficiently reduce CO_2 and syngas (mixture of CO and H_2) can be generated through CO_2/H_2O co-electrolysis for subsequent hydrocarbon fuel synthesis.

Recently, various studies have been reported to understand the electrolysis characteristics of SOEC under different conditions, but most of them were conducted only with the consideration of steady-state performance. Singh et al.[5] tested the performance of a SOEC stack in a trigeneration system, where the hydrogen yield rate of 2.1 mol/sec at 0.6 A/cm^2 was obtained. Li et al.[6] tested H_2O/CO_2 co-electrolysis between 550-750 ^{o}C and found that CH_4 could be formed at high operating voltages (> 2 V). Graves et al.[7] investigated the durability of SOEC during co-electrolysis processes and found the cathode degradation dominated at low current densities. Shi et al.[8, 9] investigated the effects of operating conditions on the co-electrolysis characteristics and reaction mechanism, they found increasing the

temperature and decreasing the flow rate could increase the conversion of CO_2. Ni et al.[10, 11] built a multi-physics model for evaluating the SOEC performance in syngas production and found that the current density is increased with inlet H_2O mole fraction. Chen et al.[12] also developed an SOEC co-electrolysis model that directly combined with the Fischer-Tropsch process, where they found the one-step process achieved a CH_4 production rate of 11.40% and a total CO_2 utilization rate of 64.1%. Xu et al.[13] studied CO_2/H_2O co-electrolysis assisted by fuel (CH_4) and found that the energy consumption was effectively reduced by the assistance of CH_4, they also developed another hybrid model consisting of multi-physics models and deep learning strategy to adjust SOEC to operate under thermal neutral conditions [14], which could help ensure its security in long-term operations. By combining with artificial neural network, Grondin et al.[15] further proposed a three-dimensional SOEC model to evaluate its electrode electrochemical behavior of SOEC with a consideration of micro-scale effects.

Regarding the transient nature of solar and wind power, several researches have been carried out to assess the operating characteristic of SOECs under partial load conditions. Petipas et al.[16] proposed a zero-dimensional model to evaluate the performance of a steady-state SOEC system operating at various power loads. Their results showed that when the system worked between 60% and 100% of the design power, SOEC operated near the thermal neutral point, while below 60%, extra heating was required. Romero et al.[17] established an SOEC system numerical model to optimize its performance at partial load conditions operated under different thermodynamic cell operational modes and found that the system could run safely in 10-100% power range with a very flat performance curve, which could enable the system coupled with high transient renewable energies. Xing et al.[18] proposed a simplified model considering the energy consumption of auxiliary equipment, which could achieve the highest energy conversion efficiency from part load to full load by coordinating operating parameters.

When fully coupled with renewable powers, the dynamic characteristic of the SOEC is dramatically changed, however, the research on the dynamic performance of the SOEC was very limited. Petipas et al.[19] performed SOEC transient tests consisting of 1,800 square waves over 140 hours with a voltage degradation rate of 5% (70 mV)/ 1000h, which paved the way for the modular operation of SOEC with intermittent renewable power. Some other works[20, 21] also showed that the degradation of SOEC was neglectable under dynamic load conditions, both in the case of steam electrolysis and co-electrolysis. Sunfire company[22] further operated the SOEC stack from 0 to 80% load in just 1ms without any degradation after 18 test cycles, proving that SOEC could possibly operate under high dynamic conditions. To save time/cost and illustrate the coupling relationship of various physical fields and providing a deep comprehension of the physical/chemical process in the SOEC, numerical studies were also conducted. Cai et al.[23] established an SOEC model to study its dynamic characteristics by replacing the changes of renewable energy with step changes of average current density, and found that when average temperature was controlled by air flow the cell potential changes required a long time to achieve the final stable state. In another study[24], they also discussed the feature of different control strategies in dynamic processes. Fogel et al.[25] proposed a 2D-FEM model to study the transient behavior of SOEC under rapid load changes, which was also achieved by the step changes of the cell current, and found that lower steam mass flow rates may increase the risk of electrode degradation. Luo et al.[26] proposed a tubular co-electrolysis dynamic model to evaluate the time constants of charge/mass/heat transfer processes. The responses to temperature/gas flow/electricity step inputs were further studied, and the effects of these input parameters on efficiency, conversion rate and H_2/CO mole ratio were analyzed. However, there was a lack of the analysis of physical fields transient behavior when the cell operating state changed from endothermic state to exothermic state. Using instantaneous wind power as input,

Wang et al.[27] built a 3D continuum model to investigate the dynamic behavior and operation strategies of SOEC, and found that air ratio could reduce SOEC temperature fluctuation. Dadak et al.[28] developed a dynamic renewable energy system based on SOEC and found that operating voltage and hydrogen generation rate increased with temperature.

Previous studies have mainly focused on using step changes in current density/stack voltage as an alternative to fluctuating renewable energy sources, with only a few articles using actual fluctuating PV/wind power as SOEC inputs. The cell operating state changes from endothermic state to exothermic state when coupled with renewable energy power source in a day. While the cell voltages with step changes are usually between OCV (Open Circuit Voltage) and thermal neutral voltage, which may underestimate the changes in temperature, H_2O/CO_2 conversion rate and output H_2/CO ratio throughout the day. Besides, these works lacked a detailed analysis of physical/chemical processes in dynamic processes, especially considering the effects of outlet H_2:CO ratio, which is vital to the downstream processes. The understanding of these characteristics can make a contribution to the control and optimization of high temperature electrolysis under renewable power source. Moreover, most of them were carried out with a constant gas supply, but not following the electrical load to maintain a high gas utilization rate, which may accelerate cell degradation under fluctuating conditions.

In order to fill the gap in the aforementioned researches, a two-dimensional rotation-axis-symmetric multi-physics model is developed to analyze the dynamic characteristic of SOEC co-electrolysis with a fluctuating PV power input. The model is validated with the steady-state experimental data on SOEC. Detailed parametric studies are carried out to analyze the complex physical/chemical processes in the SOEC with the target on a high gas utilization.

2. Model description

The 2D dynamic model of tubular SOEC is established with a full consideration of electrochemical co-reduction of CO_2 and H_2O, water gas shift reaction (WGSR), mass/momentum/heat transfer processes. Fig. 1 illustrates the working schematic of SOEC. H_2O and CO_2 are co-reduced into H_2, CO and O^{2-} on the TPB (triple-phase-boundary) by receiving electrons from an external power source. O^{2-} ions are transported to the porous anode through the highly dense electrolyte, where O_2 is produced and electrons are released through an external circuit. Electrode and electrolyte properties such as ionic, electronic conductivity and thermodynamic parameters can be found in Table 1.

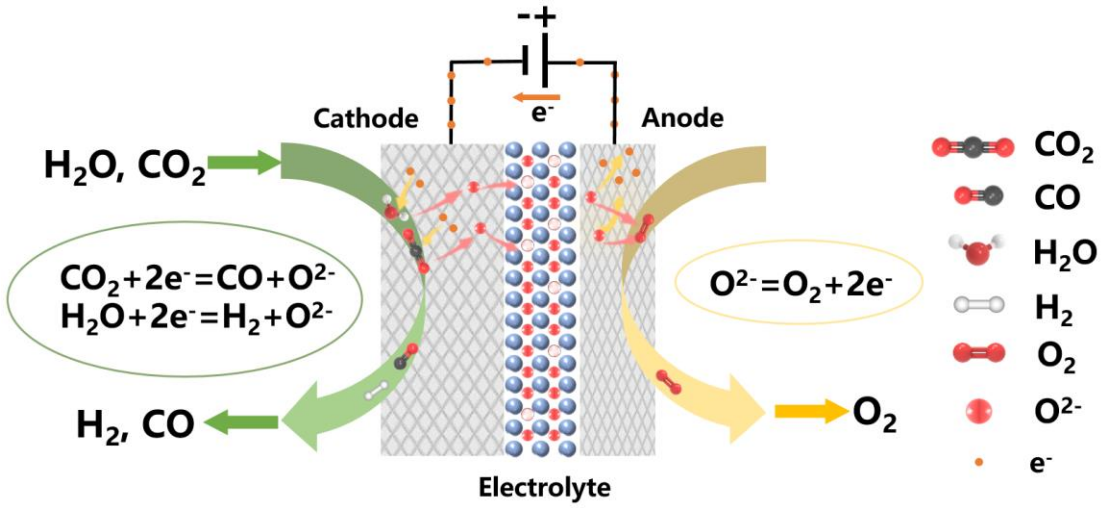

Fig. 1 Working schematic of the co-electrolysis process.

Table 1. Material parameters[14].

Parameters	Value or expression	Unit
Electronic conductivity		S/m
LSM	$4.2\times10^{7}\ exp(-1150/T)$	
Ni	$4.2\times10^{6}-1065.3T$	
Ionic conductivity		S/m

ScSZ	$6.92\times10^{4}\ exp(-9681/T)$	
YSZ	$3.34\times10^{4}\ exp(-10300/T)$	
Thickness		μm
Cathode support layer (Ni+YSZ)	760	
Cathode active layer (Ni+ScSZ)	10	
Electrolyte (ScSZ)	10	
Anode active layer (LSM+ScSZ)	15	
Heat Conductivity		W/(m·K)
Cathode	6.23	
Electrolyte	2.7	
Anode	9.6	
Heat Capacity		J/(kg·K)
Cathode	390	
Electrolyte	300	
Anode	420	
Density		kg/m^3
Cathode	6870	
Electrolyte	2000	

Anode	6570

2.1 Model assumption

(1) Reaction sites distribute evenly in the electrodes as all the materials are supposed to be well mixed in the preparation of SOEC. The ionic and electronic charge transfer processes occur at TPB.

(2) H_2O and CO_2 share the reaction sites.

(3) CO_2, CO, H_2O, H_2, O_2 and N_2 in the model are regarded as ideal gases due to the high operating temperature.

(4) Radiative heat transfer loss is ignored.

2.2 Governing equations

The dynamic SOEC model employs a continuum microscale porous electrode model coupling the electrochemical reactions in electrodes, WGSR in porous cathode, and gas diffusion effected by the electrode microstructures. Gas flow in channels can be determined by incompressible N-S equation. While in porous layers, the momentum conservation equation is further corrected by introducing the Darcy's Law term. Heat production/consumption from electrochemical/chemical reactions and various overpotential losses are also considered. The governing equations used in this model are listed in Table 2, and the detailed description is presented in supporting information.

Table 2 Governing equations used in this model.

Electrochemical reaction model	
$V = E_{eq} + \eta_{act} + \eta_{o\square mic}$	Required potential

$E_{\mathrm{eq,H_2O}} = E^0_{\mathrm{eq,H_2O}} + \frac{\mathrm{RT}}{2F} ln \left[\frac{P^{L,C}_{H_2} \left(P^{L,A}_{O_2}\right)^{1/2}}{P^{\mathrm{L,C}}_{H_2O}} \right]$	Equilibrium potentials of H_2O
$E^0_{H_2O} = 1.253 - 0.00024516T\ (V)$	Standard potential of H2O
$E_{\mathrm{eq,CO_2}} = E^0_{\mathrm{eq,CO_2}} + \frac{\mathrm{RT}}{2F} ln \left[\frac{P^{L,C}_{CO} \left(P^{L,A}_{O_2}\right)^{1/2}}{P^{\mathrm{L,C}}_{CO_2}} \right]$	Equilibrium potentials of CO_2
$E^0_{CO_2} = 1.46713 - 0.0004527T\ (V)$	Standard potential of CO_2
$\nabla \cdot (-\sigma_l \nabla \emptyset_l) = i$	Charge balance for ironic phase
$\nabla \cdot (-\sigma_s \nabla \emptyset_s) = i$	Charge balance for electron phase
$i = i_0 \left\{ exp\left(\frac{\alpha \mathrm{nF} \eta_{\mathrm{act}}}{\mathrm{RT}}\right) - exp\left(-\frac{(1-\alpha)\mathrm{nF}\eta_{\mathrm{act}}}{\mathrm{RT}}\right) \right\}$	Butler-Volmer equation
Mass/momentum conservation	
$N_i = -\frac{1}{RT}\left(\frac{B_0 y_i P}{\mu}\frac{\partial P}{\partial z} - D^{eff}_i \frac{\partial (y_i P)}{\partial z}\right)(i = 1, \dots, n)$	Gas diffusion model
$D^{eff}_i = (\frac{1}{D^{eff}_{im}} + \frac{1}{D^{eff}_{ik}})^{-1}$	Effective diffusivity
$\rho \frac{\partial u}{\partial t} + \rho u \nabla u = -\nabla P + \nabla \mu \left[(\nabla u + (\nabla u)^T) - \frac{2}{3}\mu \nabla u \right] - \frac{\varepsilon \mu u}{\kappa}$	Momentum conservation with Darcy's term
Heat transfer model	
$(\rho C_p)_{eff} \frac{\partial T}{\partial t} + \rho C_{p,g} U \nabla T + \nabla(-\lambda_{eff} \nabla T) = Q$	Energy balance equation
$\lambda_{eff} = (1-\varepsilon)\lambda_s + \varepsilon \lambda_g$	Effective heat conductivity
$(\rho C_p)_{eff} = (1-\varepsilon)\rho_s C_{p,s} + \varepsilon \rho_g C_{p,g}$	
Chemical reaction model	
$CO + H_2O \leftrightarrow CO_2 + H_2$	Water gas shift reaction
$R_{WGSR} = k_{sf}\left(P_{H_2O} P_{co} - \frac{P_{H_2} P_{CO_2}}{K_{ps}}\right)$	Reaction rate
$k_{sf} = 0.0171\, exp\left(\frac{-103191}{RT}\right)$	Reaction rate constant

$K_{ps} = exp(-0.2935Z^3 + 0.6351Z^2 + 4.1788Z + 0.3169)$	Reaction equilibrium constant
$Z = \frac{1000}{T} - 1$	Mean coordination number

2.3 Boundary conditions

The gas temperature, standard gas flow rates and mole fractions are given at the entrances of two channel, and the outlet pressure condition is set to standard atmospheric pressure. The outer walls are set as adiabatic boundary condition. At the anode/channel interface and the cathode/channel interface, the electric potentials are designated as operating potential and electrical ground, respectively. Other boundaries are considered electric-insulating.

2.4 Model solution

The governing equations summarized above are solved through the finite element method in the COMSOL Multiphysics software. The simulation results include the distributions of temperature, potential, current density, gas mole fraction and others.

2.5 Model validation input profile

Fig. 2a shows the comparison results of current voltage characteristics between steady-state model and experimental data for co-electrolysis[9]. The operation conditions are listed in Table S1. The simulation result consistent with the experimental result validates the accuracy of the model.

In the previous literatures, square wave-like step changes in the operating voltage or average current

density have been usually employed to simulate the intermittent input of renewable energy power, which cannot precisely describe its actual fluctuation features. In this paper, the profile of input power is acquired using a real-time PV power station data during a sunny spring day around the vernal equinox day in Zhejiang Province, China with a sampling interval of 5 min. By limiting the maximum operating voltage (1.5 V) and minimum operating voltage (0.95 V) of the SOEC, we can calculate the corresponding input voltage profile (Fig. 2b) regarding a constant-current output from the PV power station.

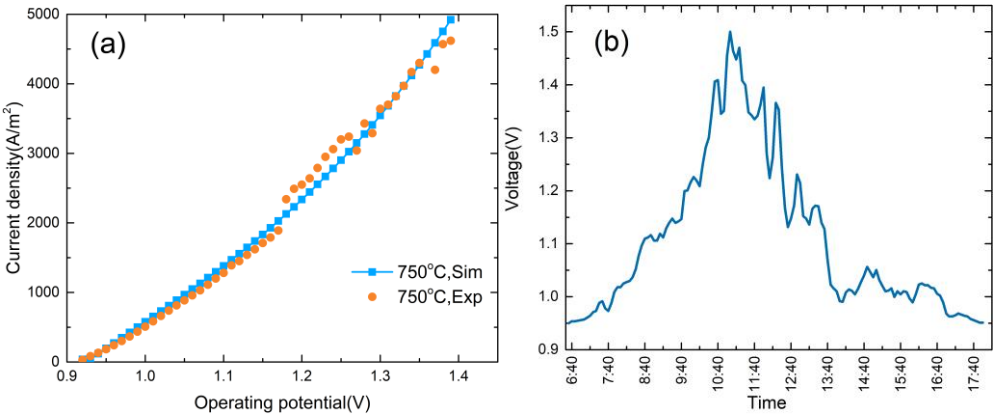

Fig. 2 (a) Model validation for SOEC, (b) profile of fluctuating voltage input to SOEC.

3. Results and discuss

3.1. Effects of cathode inlet gas composition

H_2O and CO_2 have very different electrochemical activities and there also exists water gas shift reaction that affects the conversion among these reactants. Therefore, the cathode inlet gas composition is not only vital to the gas composition at the outlet, but also affects the other cell performances such as the heat generation, temperature distribution and conversion rate. In this section, the effects of cathode inlet gas composition are studied with detailed operating conditions shown in Table S2.

The current density fluctuated along with the changing voltage, where a high inlet H_2O mole fraction presented a much larger amplitude than that with a low H_2O fraction, as shown in Fig. 3a. At

11:00, the current density of 0.8-H_2O case reached about 2.4 A/cm^2, which was 66% higher than that at 0.2-H_2O case. Despite the changing of voltage and current density, the conversion rate of H_2O was always larger than that of CO_2 at different H_2O/CO_2 ratios (Fig. 3b). The smallest difference (~10%) occurred at 11:00 of the 0.8-H_2O case, while the largest difference (~80%) occurred around 9:00/14:00 of the 0.5 mole fraction case. A similar tendency was also observed in Fig. 3c, where the outlet H_2/CO ratio decreased by about 30% from 9:40 to 11:00 at the 0.8-H_2O case, indicating the H_2O mole fraction should be increased to maintain a high H_2/CO ratio at high operating voltages. These phenomena were caused by the competition in the electrochemical and chemical conversions of H_2O and CO_2. On one hand, H_2O had a higher electrochemical chemical activity than CO_2 and thus dominating the electrochemical reduction reaction. On the other hand, the direction of WGSR was affected by the temperature, where a higher temperature favors the formation of CO by consuming H_2. As shown in Fig. 3d, a high CO_2 mole fraction (low H_2O case) could help inhibit average temperature fluctuation, where the maximum temperature difference was decreased from 110 K to 57 K with the inlet CO_2 mole fraction increasing from 0.2 to 0.8.

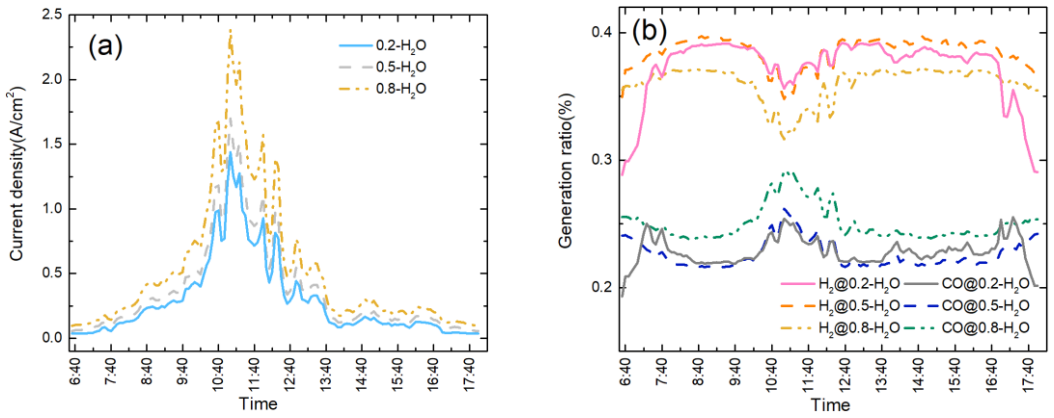

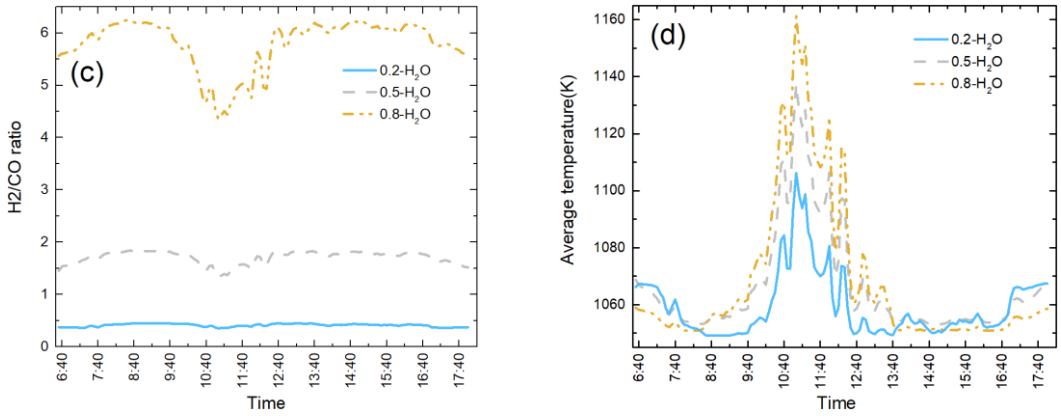

Fig. 3 Effect of inlet H_2O mole fraction change on the dynamic performance of SOEC at 1073K and 60% total gas utilization. Dynamic response of (a) current density, (b) generation ratio, (c) H_2/CO ratio, and (d) average temperature.

Breakdowns of heat sources at two typical nodes (8:40 & 11:00) were further presented in Fig. 4a & 4b. It should be noted the negative value represents heat absorption. The overall heat generation value was negative in the morning and became positive at noon due to the increase of applied voltage. Entropy changes dominated the heat sink especially at asymmetrical cases (0.2 & 0.8), and WGSR played an important role at the 0.5-H_2O case especially at 8: 40, where enough H_2O supply ensured a high electrochemical activity and a relative high CO_2 mole fraction accelerated the generation of CO. With the increase of H_2O mole fraction, a higher electrochemical activity could be expected and heat generations from the activation overpotential loss and the ohmic overpotential loss were significantly increased. As further illustrated in Fig. 4c & 4d, cell temperature decreased along with the flow direction in the morning, and the largest (most negative) temperature gradient (-7.09 K/cm) occurred in the middle of the cell at the 0.2-H_2O case. As time went, the cell temperature became rising along the flow direction and the largest temperature gradient reached 55 K/cm near the inlet area at the 0.8-H_2O case. To avoid a large temperature gradient, a relatively high H_2O mole fraction is suggested at low voltages (morning

case) and a low H_2O mole fraction is suggested at high voltages (noon case).

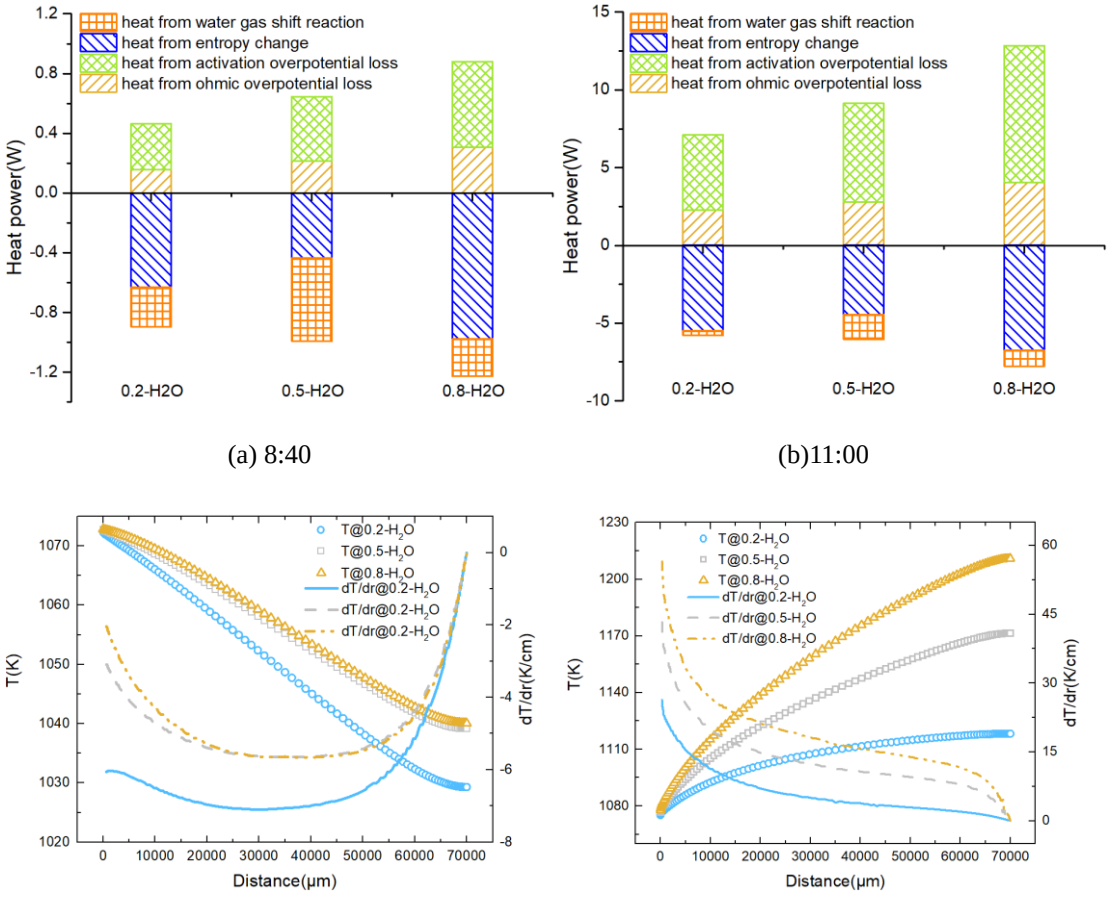

Fig. 4 (a) & (b) Breakdowns of heat power from different process in the cell, (c) & (d) diagrams of temperature and temperature gradient in length direction at the interface of cathode and electrolyte.

3.2. Effects of inlet gas temperature

Inlet gas temperature is a key factor on the kinetics of the chemical and electrochemical reactions, thus not only affects the I-V characteristics, but also affects its exothermic/endothermic status. The effects of inlet gas temperature are studied in this section, and the related operating conditions are presented in Table S3.

The current density was increased at a higher inlet gas temperature, as shown in Fig. 5a. At 11:00, the current density of 1123K case reached about 2.7 A/cm^2, which was approximately three times that of 1023K case. As can be seen from Fig. 5b, H_2O conversion increased with the increasing of inlet gas temperature. However, when the working voltage exceeded 1.2V at 9:50 am, the effect of inlet gas temperature on the H_2O conversion was negligible. H_2/CO ratio had the same trend with H_2O conversion, as shown in Fig. 5c. At 8:40, output H_2/CO ratio of 1123K case reached about 1.91, which was 12% higher than that at 1023K case. At noon, the difference was only 4 %, indicating the inlet gas temperature had little effect on H_2/CO ratio at high operating voltages (>1.2V). It could also be found from Fig. 5d that the maximum temperature difference along the whole day increased with inlet gas temperature, which is 68K, 84K and 100K respectively.

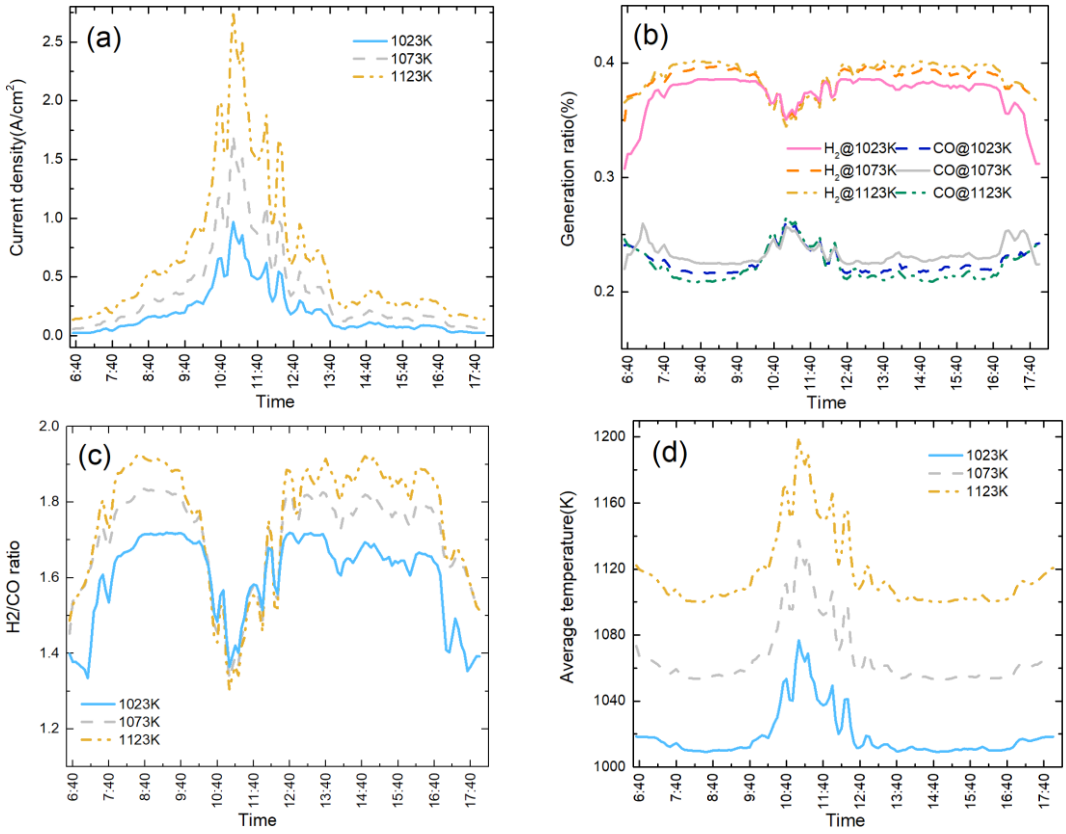

Fig. 5 Effects of inlet gas temperature change on the dynamic performance of SOEC at 50% inlet H_2O

mole fraction and 60% total gas utilization. Dynamic response of (a) current density, (b) generation ratio, (c) H_2/CO ratio, and (d) average temperature.

As shown in Fig. 6a & 6b for the breakdown of heat source, temperature had an important effect on WGSR rate. Heat from WGSR of 1123K case was -1.38 W and -3.9 W at 8:40 and 11:00, respectively, which was both approximately seven times that of 1023K case. With the increase of inlet gas temperature, a higher electrochemical activity could be expected and heat generations from the activation overpotential loss and the ohmic overpotential loss were significantly increased. As shown in Fig. 6c & 6d, cell outlet temperature of 1123K case was reduced by 35K at 8:40 and increased by 108K at 11:00, which was 44% and 30% higher than that at 1023K case, respectively. The maximum temperature gradient occurred at 1123K case whether in the morning endothermic stage or at the noon exothermic stage. It was worth noting that there is little difference in temperature gradient in the middle and outlet of the cell among different inlet gas temperature cases at 11:00.

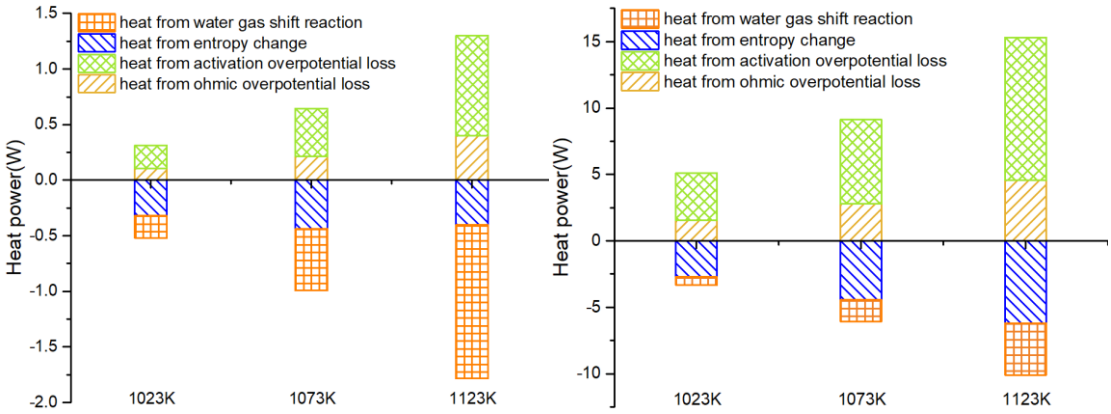

(a) 8:40 (b) 11:00

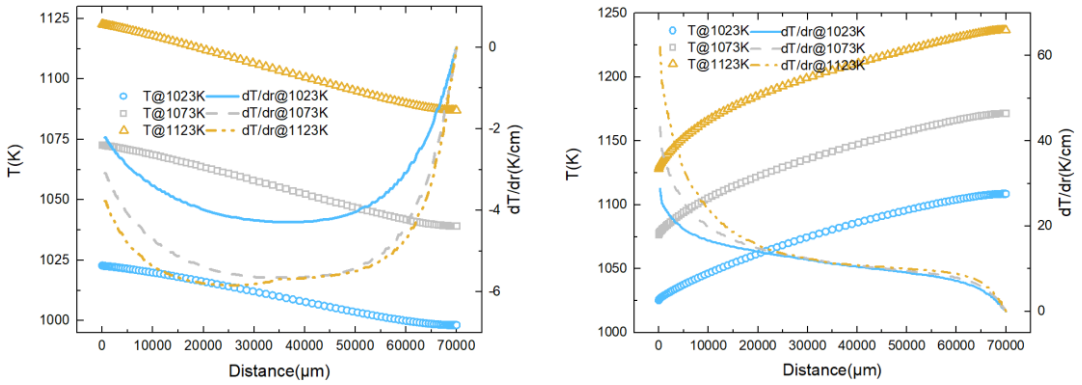

(c) 8:40 (d) 11:00

Fig. 6 (a) & (b) Breakdowns of heat power from different process in the cell, (c) & (d) diagram of temperature and temperature gradient in length direction at the interface of cathode and electrolyte.

3.3. Effects of cathode gas utilization rate

A high gas utilization rate is desired in the practical operation of SOECs, but a thoroughly utilization will cause "reactant starvation". For this concern, the utilization rate should be optimized to achieve economic benefits in the long-term operating. In this section, the effects of cathode gas utilization rate are studied and related operating conditions at different utilization rates are listed in Table S4.

Different total gas utilization had little influence on current density of SOEC, which reached about 1.7 A/cm^2 at 11:00, as shown in Fig. 7a. A high total gas utilization resulted in a large H_2O and CO_2 conversion, but the H_2/CO ratio was lower, as shown in Fig. 7b & 7c. Output H_2/CO ratio at 60% case was on average 10% higher than that at 80% case during the day. It was suggested that 60% total gas utilization should be selected as the operating condition in order to ensure a high H_2/CO ratio. Total gas utilization also had little influence on average temperature fluctuation, where the maximum temperature difference was about 90 K, as shown in Fig. 7d.

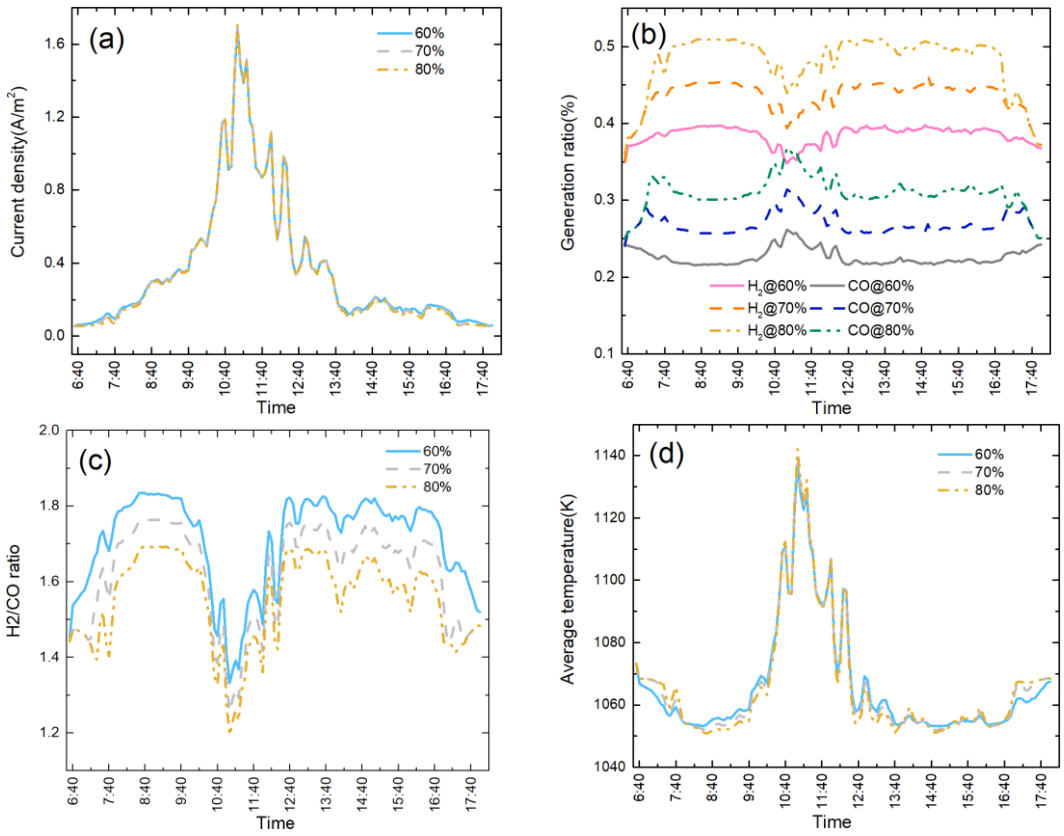

Fig. 7 Effects of cathode total gas utilization change on the dynamic performance of SOEC at 50% inlet H_2O mole fraction and 1073K inlet gas temperature. Dynamic response of (a) current density, (b) generation ratio, (c) H_2/CO ratio, and (d) average temperature.

The heat from different process at two typical nodes (8:40 & 11:00) was roughly the same under different gas utilization, as shown in Fig 8a & 8d. WGSR enthalpy changes dominated the heat sink in the morning, while entropy changes dominated the heat sink at noon. As further illustrated in Fig. 8c & 8d, there was a slight difference in the outlet temperature at different gas utilization cases. In the morning, there was little difference in the temperature gradient at the outlet of the cell at different gas utilization cases, and the maximum temperature gradient (-6.52 K/cm) occurred in the middle of the cell at the 80% case. However, at noon, the temperature gradient was almost the same at any locations of the cell, which reached the max value of 42 K/cm near the inlet area. To avoid a large temperature gradient, a relative low gas utilization is suggested at low voltages.

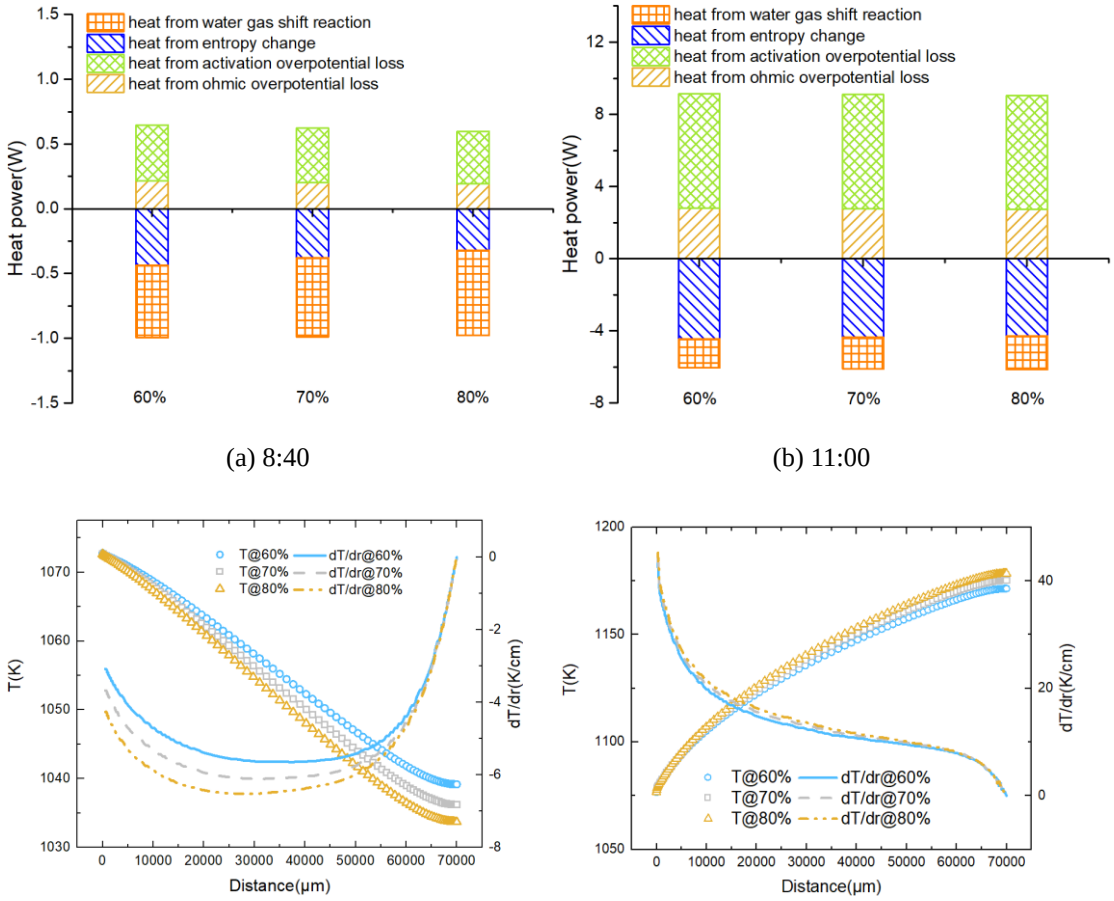

(a) 8:40 (b) 11:00

(c) 8:40 (d) 11:00

Fig. 8 (a) & (b) Breakdowns of heat power from different process in the cell, (c) & (d) diagrams of temperature and temperature gradient in length direction at the interface of cathode and electrolyte.

4. Conclusion

In summary, a 2D numerical model has been developed to analyze dynamic performances of SOEC co-electrolysis applied with real fluctuating photovoltaic inputs. Chemical/electrochemical reaction, mass/momentum transport and heat transfer processes were fully considered and parametric studies were conducted with a particular attention on the performances of heat generation, temperature gradient distribution and H_2/CO ratio at the outlet.

It is found that the inlet gas mole fraction significantly affects the transient behavior of SOEC. A high CO_2 mole fraction helps inhibit average temperature fluctuation, where the maximum temperature difference can be decreased from 110 K to 57 K with the inlet CO_2 mole fraction increasing from 0.2 to 0.8. Besides, the most negative temperature gradient (-7 K/cm) occurs in the middle of the cell at the 0.2-H_2O case in the morning, while the largest temperature gradient can reach 55 K/cm near the inlet area at the 0.8-H_2O case at noon. Moreover, the outlet H_2/CO ratio decreases by about 30% from 9:40 to 11:00 at the 0.8-H_2O case. The inlet H_2O mole fraction should thus be compromised to maintain a high H_2/CO ratio to avoid a large temperature gradient at high voltages. Inlet gas temperature is another important role that affects the output H_2/CO ratio of the cell. A high inlet gas temperature helps increase the outlet H_2/CO ratio at small voltages (< 1.2 V), but has little effect on H_2/CO ratio at high voltages. The maximum temperature gradient occurs at 1123K cases in both the endothermic stage (morning) and the exothermic stage (noon). To maintain the output H_2/CO ratio while avoiding large temperature gradients, a relatively high inlet gas temperature is suggested at low voltages. As for the effects of total gas utilization, it is found that the output H_2/CO ratio at 60% case is averagely 10% higher than that at 80% case during the whole day, and a relative low gas utilization is suggested at low voltages.

The understanding of these characteristics can guide the efficient conversion of fluctuating renewable power and optimization of high temperature electrolysis at transient conditions.

Acknowledgement

The authors gratefully acknowledge the support from the Zhejiang Provincial Key R&D Program (NO.2022C01043), the Zhejiang Provincial Natural Science Foundation (NO.LR20E060001). M.NI also

thanks the grants (Project Number: PolyU 152064/18E and N_PolyU552/20) from Research grant Council, University Grants Committee, Hong Kong SAR.

References

[1].Sinsel, S.R., R.L. Riemke, and V.H. Hoffmann, Challenges and solution technologies for the integration of variable renewable energy sources—a review. Renewable energy, 2020. 145: p. 2271-2285.
[2].Edwards, R.L., C. Font-Palma, and J. Howe, The status of hydrogen technologies in the UK: A multi-disciplinary review. Sustainable energy technologies and assessments, 2021. 43: p. 100901.
[3].Hauch, A., et al., Recent advances in solid oxide cell technology for electrolysis. Science (American Association for the Advancement of Science), 2020. 370(6513): p. 186.
[4].Gahleitner, G., Hydrogen from renewable electricity: An international review of power-to-gas pilot plants for stationary applications. International journal of hydrogen energy, 2013. 38(5): p. 2039-2061.
[5].Raj Singh, U., A. Sai Kaushik, and S. Sekhar Bhogilla, A novel renewable energy storage system based on reversible SOFC, hydrogen storage, Rankine cycle and absorption refrigeration system. Sustainable energy technologies and assessments, 2022. 51.
[6].Li, W., et al., Performance and methane production characteristics of H2O–CO2 co-electrolysis in solid oxide electrolysis cells. International journal of hydrogen energy, 2013. 38(25): p. 11104-11109.
[7].Graves, C., S.D. Ebbesen, and M. Mogensen, Co-electrolysis of CO2 and H2O in solid oxide cells: Performance and durability. Solid state ionics, 2011. 192(1): p. 398-403.
[8].Li, W., et al., Elementary reaction modeling of solid oxide electrolysis cells: Main zones for heterogeneous chemical/electrochemical reactions. Journal of power sources, 2015. 273: p. 1-13.
[9].Luo, Y., et al., Comprehensive modeling of tubular solid oxide electrolysis cell for co-electrolysis of steam and carbon dioxide. Energy (Oxford), 2014. 70: p. 420-434.
[10].Ni, M., An electrochemical model for syngas production by co-electrolysis of H2O and CO2. Journal of power sources, 2012. 202: p. 209-216.
[11].Ni, M., 2D thermal modeling of a solid oxide electrolyzer cell (SOEC) for syngas production by H2O/CO2 co-electrolysis. International journal of hydrogen energy, 2012. 37(8): p. 6389-6399.
[12].Chen, L., F. Chen, and C. Xia, Direct synthesis of methane from CO2-H2O co-electrolysis in tubular solid oxide electrolysis cells. Energy & environmental science, 2014. 7(12): p. 4018-4022.
[13].Xu, H., et al., Modeling of CH4-assisted SOEC for H2O/CO2 co-electrolysis. International journal of hydrogen energy, 2016. 41(47): p. 21839-21849.
[14].Xu, H., et al., Enabling thermal-neutral electrolysis for CO2-to-fuel conversions with a hybrid deep learning strategy. Energy conversion and management, 2021. 230: p. 113827.
[15].Grondin, D., et al., Solid oxide electrolysis cell 3D simulation using artificial neural network for cathodic process description. Chemical engineering research & design, 2013. 91(1): p. 134-140.
[16].Petipas, F., A. Brisse, and C. Bouallou, Model-based behaviour of a high temperature electrolyser system operated at various loads. Journal of power sources, 2013. 239: p. 584-595.
[17].Sanz-Bermejo, J., et al., Part load operation of a solid oxide electrolysis system for integration with renewable energy sources. International journal of hydrogen energy, 2015. 40(26): p. 8291-8303.
[18].Xing, X., et al., Optimization of hydrogen yield of a high-temperature electrolysis system with

coordinated temperature and feed factors at various loading conditions: A model-based study. Applied energy, 2018. 232: p. 368-385.
[19].Petipas, F., et al., Transient operation of a solid oxide electrolysis cell. International journal of hydrogen energy, 2013. 38(7): p. 2957-2964.
[20].Schefold, J., et al., 80,000 current on/off cycles in a one year long steam electrolysis test with a solid oxide cell. International journal of hydrogen energy, 2020. 45(8): p. 5143-5154.
[21].Rao, M., X. Sun, and A. Hagen, Durability of solid oxide electrolysis stack under dynamic load cycling for syngas production. Journal of power sources, 2020. 451: p. 227781.
[22].Posdziech, O., K. Schwarze, and J. Brabandt, Efficient hydrogen production for industry and electricity storage via high-temperature electrolysis. International journal of hydrogen energy, 2019. 44(35): p. 19089-19101.
[23].Cai, Q., N.P. Brandon, and C.S. Adjiman, Modelling the dynamic response of a solid oxide steam electrolyser to transient inputs during renewable hydrogen production. Frontiers of energy and power engineering in China, 2010. 4(2): p. 211-222.
[24].Cai, Q., C.S. Adjiman, and N.P. Brandon, Optimal control strategies for hydrogen production when coupling solid oxide electrolysers with intermittent renewable energies. Journal of power sources, 2014. 268: p. 212-224.
[25].Fogel, S., H. Kryk, and U. Hampel, Simulation of the transient behavior of tubular solid oxide electrolyzer cells under fast load variations. International journal of hydrogen energy, 2019. 44(18): p. 9188-9202.
[26].Luo, Y., et al., Dynamic electro-thermal modeling of co-electrolysis of steam and carbon dioxide in a tubular solid oxide electrolysis cell. Energy (Oxford), 2015. 89: p. 637-647.
[27].Wang, Y., A. Banerjee, and O. Deutschmann, Dynamic behavior and control strategy study of CO2/H2O co-electrolysis in solid oxide electrolysis cells. Journal of power sources, 2019. 412: p. 255-264.
[28].Dadak, A., M. Mehrpooya, and A. Kasaeian, Design and development of an innovative integrated structure for the production and storage of energy and hydrogen utilizing renewable energy. Sustainable energy technologies and assessments, 2021. 45: p. 101123.

List of figures:

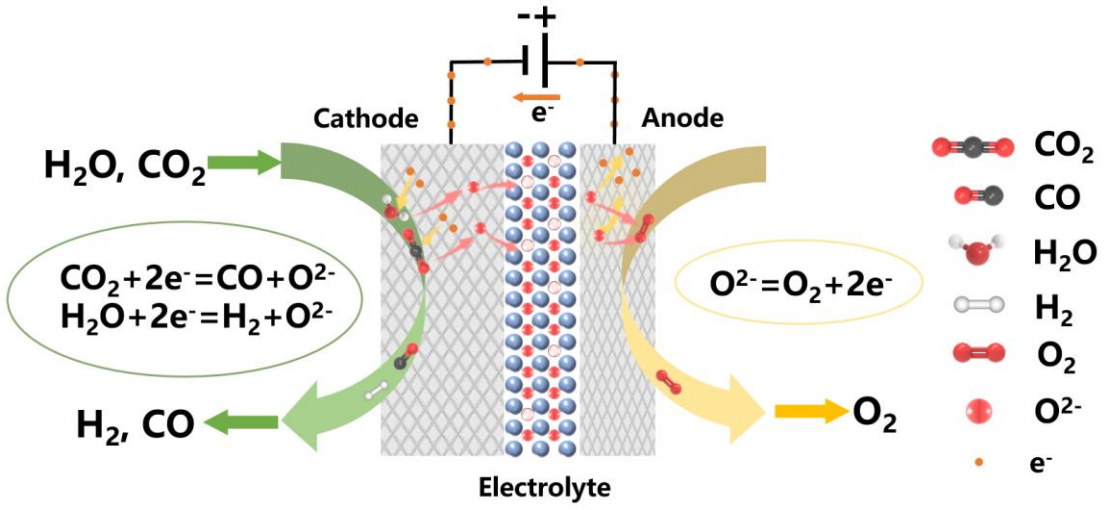

Fig. 1 Working schematic of the co-electrolysis process.

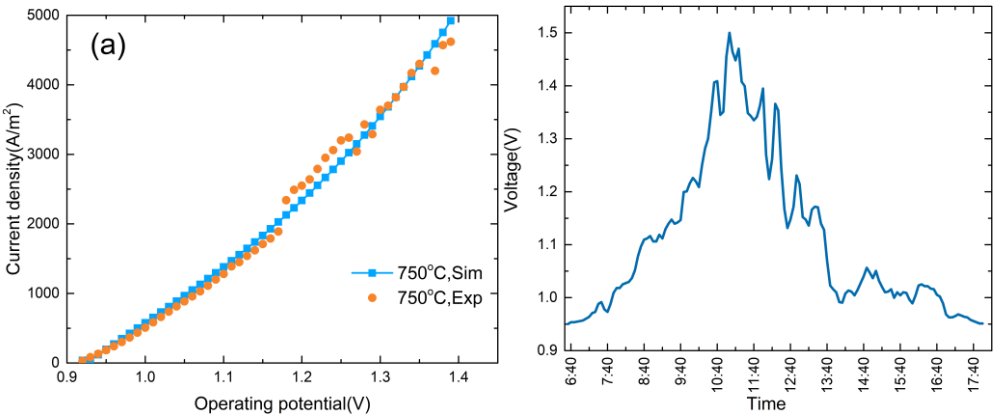

Fig. 2 (a) Model validation for SOEC, (b) profile of fluctuating voltage input to SOEC.

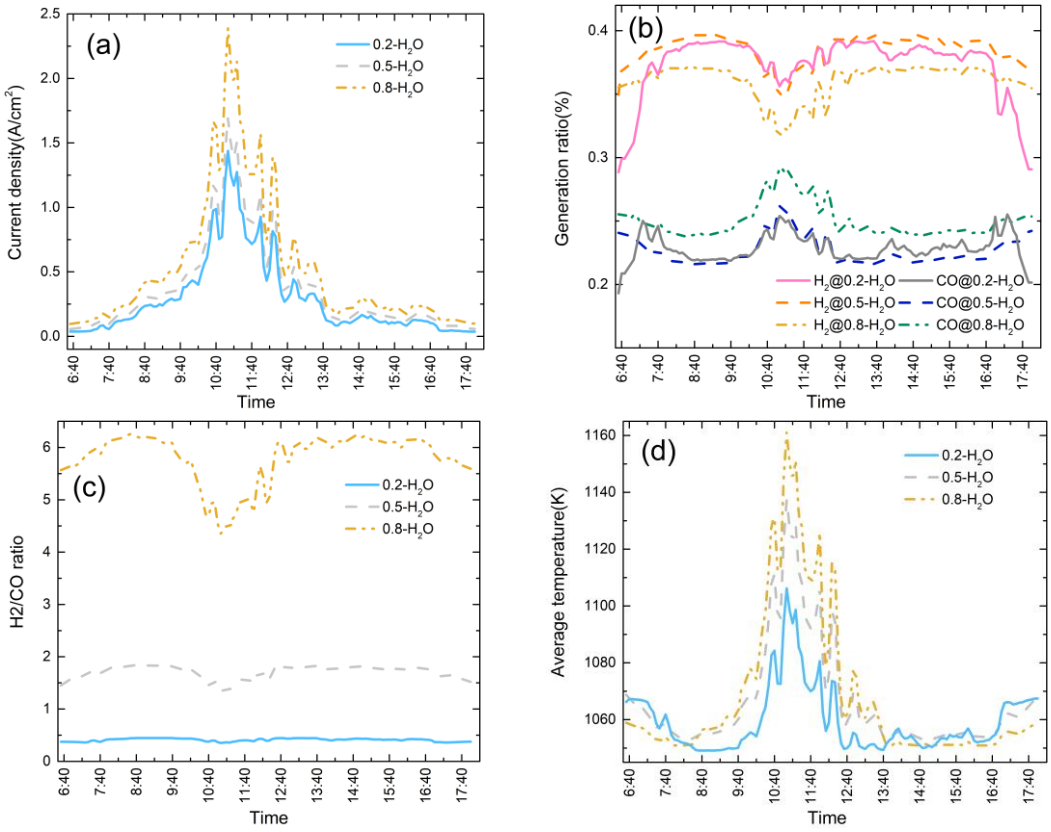

Fig. 3 Effect of inlet H_2O mole fraction change on the dynamic performance of SOEC at 1073K and 60% total gas utilization. Dynamic response of (a) current density, (b) generation ratio, (c) H_2/CO ratio, and (d) average temperature.

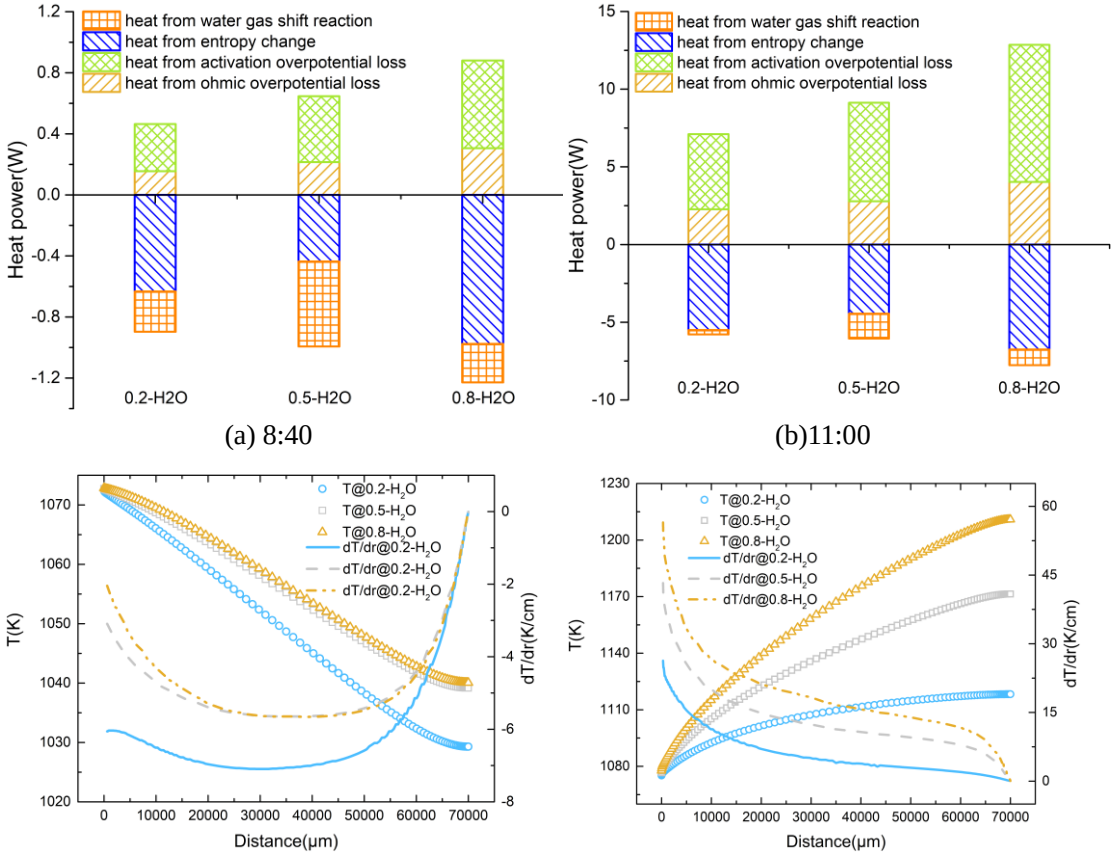

Fig. 4 (a) & (b) Breakdowns of heat power from different process in the cell, (c) & (d) diagrams of temperature and temperature gradient in length direction at the interface of cathode and electrolyte.

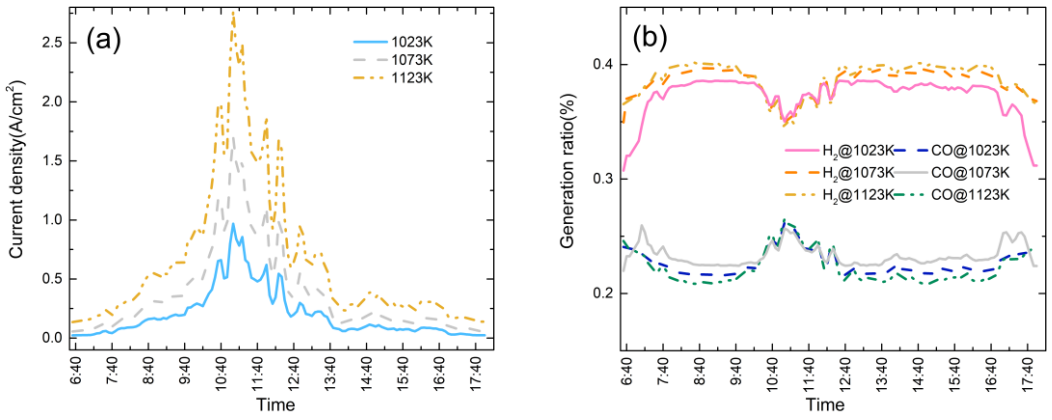

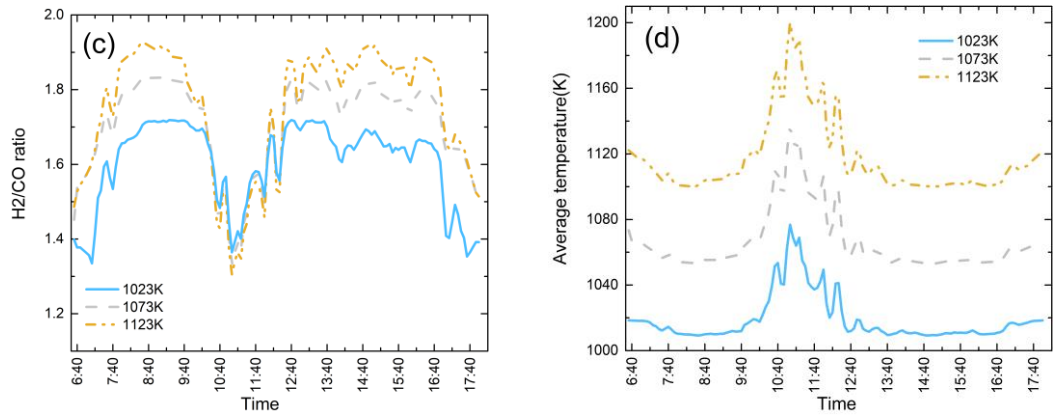

Fig. 5 Effects of inlet gas temperature change on the dynamic performance of SOEC at 50% inlet H_2O mole fraction and 60% total gas utilization. Dynamic response of (a) current density, (b) generation ratio, (c) H_2/CO ratio, and (d) average temperature.

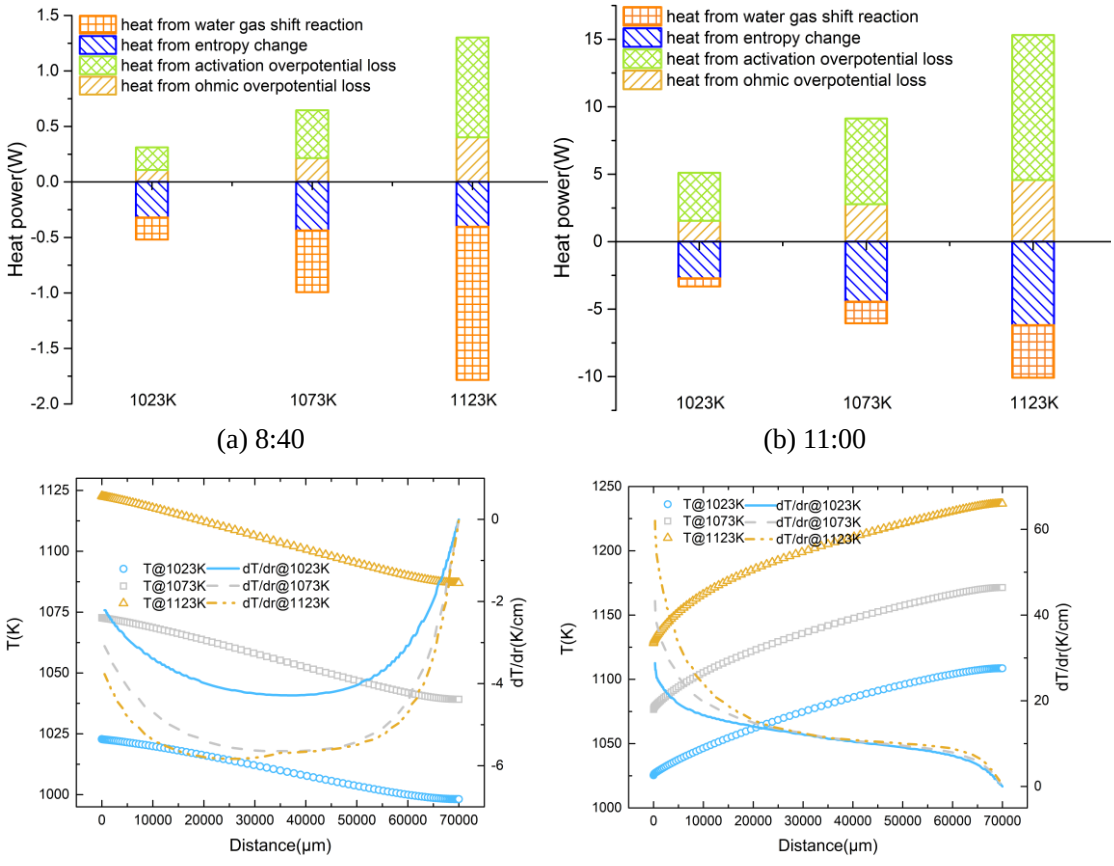

(c) 8:40 (d) 11:00

Fig. 6 (a) & (b) Breakdowns of heat power from different process in the cell, (c) & (d) diagram of temperature and temperature gradient in length direction at the interface of cathode and electrolyte.

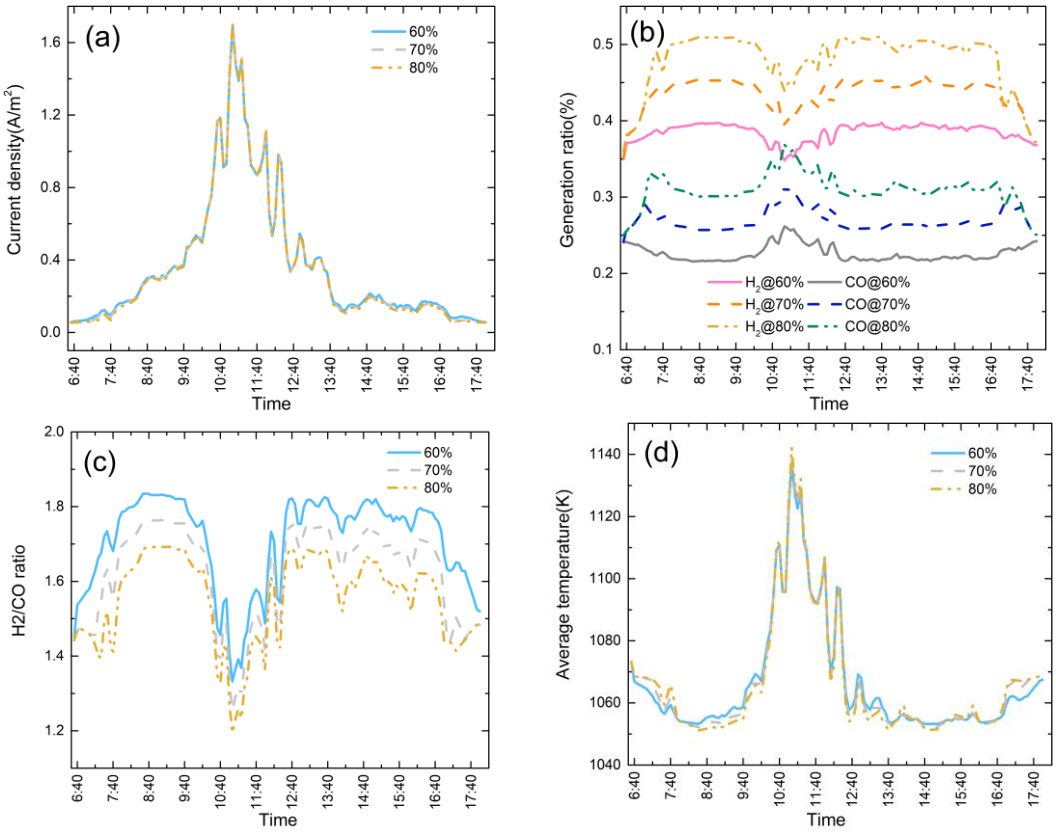

Fig. 7 Effects of cathode total gas utilization change on the dynamic performance of SOEC at 50% inlet H_2O mole fraction and 1073K inlet gas temperature. Dynamic response of (a) current density, (b) generation ratio, (c) H_2/CO ratio, and (d) average temperature.

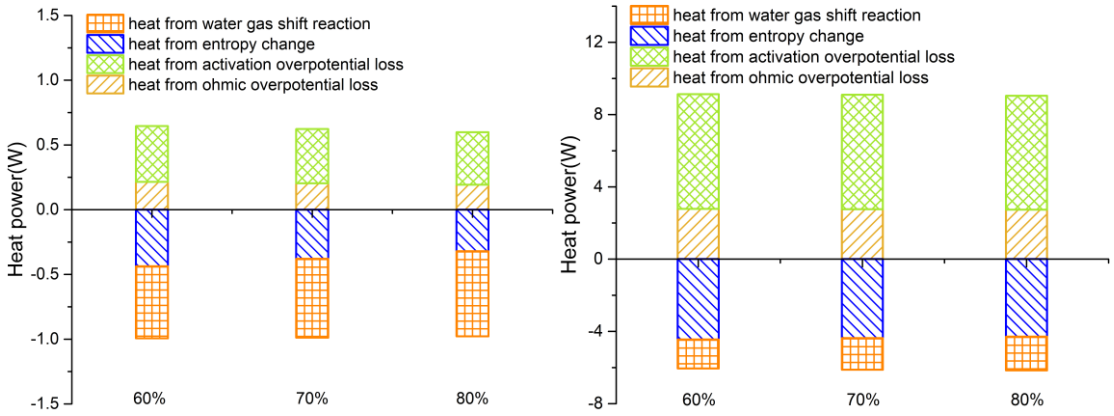

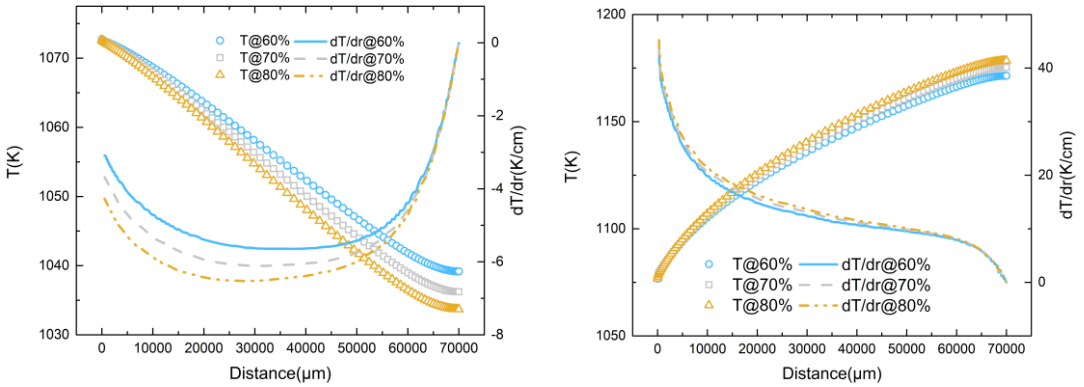

(c) 8:40 (d) 11:00

Fig. 8 (a) & (b) Breakdowns of heat power from different process in the cell, (c) & (d) diagrams of temperature and temperature gradient in length direction at the interface of cathode and electrolyte.